Neutron-scattering studies of phonons in disordered cubic zirconia at elevated temperatures

D. W. Liu,* C. H. Perry, and A. A. Feinberg†
Department of Physics, Northeastern University, Boston, Massachusetts 02115

R. Currat
Institute Laue-Langevin, 38042 Grenoble, France
(Received 6 July 1987)

Inelastic-neutron-scattering studies of cubic zirconia at elevated temperatures (300–1700 K) showed well-defined LA and TA phonons but no optical-phonon branches were observed, confirming earlier reported reduced Raman scattering data. The LA and TA phonons were observed to broaden with a q^2 dependence. The elastic constants C_{11}, C_{12}, and C_{44} were derived from the dispersion data at room temperature and at elevated temperatures. The frequency distribution of one phonon density of states was generated from the dispersion relation and was found to be in reasonable agreement with the observed Raman spectrum. Also diffuse-elastic-scattering measurements were taken and showed broad intensity peaks in reciprocal space. The scattering and the phonon linewidths showed little temperature dependence; intrinsic defects and anharmonicity dominate the damping mechanism. The unobserved optical branches were obtained by the best fit to the experimentally determined acoustic branches, based upon a rigid-ion-model calculation. Static deformations of the oxygen sublattice due to oxygen vacancies are mainly responsible for the data observed.

I. INTRODUCTION

Zirconium oxide (ZrO_2) is at present one of the most important and widely used high-temperature materials. The number of applications continues to grow with fast advances in technology.[1,2] The phonon modes in ZrO_2·Y_2O_3 mixed crystals with 0–20 wt. % Y_2O_3 have been studied from 4–1600 K using infrared reflection and Raman spectroscopic techniques.[3–5] The spectra uniquely described the structural modifications, the phase transitions, and the mixed-phase regions as the Y_2O_3 content and the temperature were varied. At room temperature samples with <9 wt. % occur as multidomain single crystals exhibiting monoclinic (M), tetragonal (T), and mixed ($M+T$) phases. Between 9 and 12 wt. % mixed tetragonal and cubic phases can be distinguished.[5] Above 12 wt. % the crystals possess the cubic fluorite structure; both Laue and powder x-ray diffraction analyses indicate that the zirconium sublattice has a perfect fcc structure. However, the translational disorder introduced by vacancies in the oxygen sublattice causes breakdown of selection rules, and the reduced Raman spectra essentially represent the frequency distribution of the phonon density of states.[3,6,7] Previous studies of the lattice dynamics of many crystals with the fluorite structure have concentrated on the alkali earth fluorite and chlorides. Of the oxides, only UO_2 has been investigated in any detail.[8] Axe and Pettit also briefly discussed ThO_2,[9] although no dispersion data are available. In recent years it has been possible to grow large (~ 20 cm^3), clear, gem-quality fluorite crystals of cubic zirconia by a cold crucible directional solification process known as skull melting[2,10] (samples supplied by Ceres Corporation, Waltham, Massachusetts). To compare ZrO_2 with these oxides we have concentrated on materials containing both 15 and 20 wt. % Y_2O_3. The mass defect is virtually negligible al-

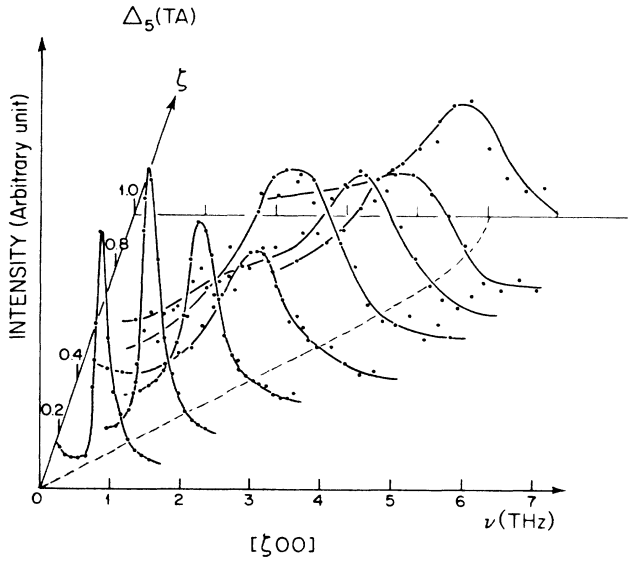

FIG. 1. The results of constant-Q scan for ZrO_2–20 wt. % Y_2O_3 TA phonons along the [ζ00] direction. The phonon line shapes as a function of ν (ζ in Fig. 2) were assumed to be Lorentzian in form and were fitted for each scan as indicated by solid lines. The projection of these peaks on the ν-ζ plane are shown by dashed lines for the TA branch.

 ©1987 The American Physical Society

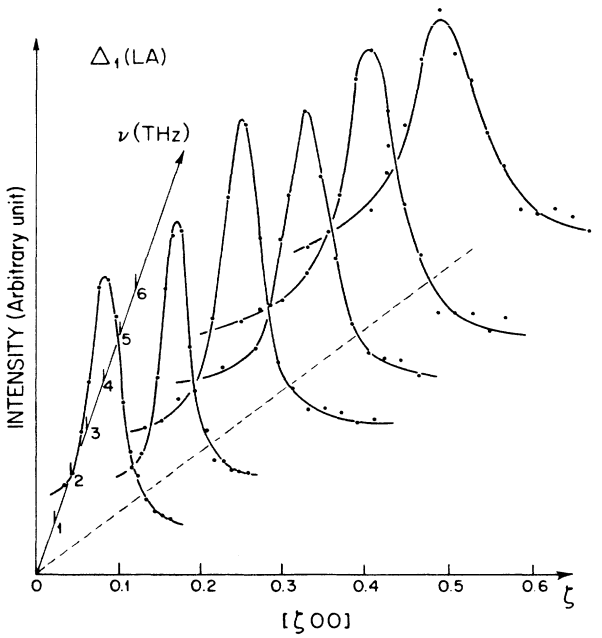

FIG. 2. The results of constant energy scans for ZrO_2–20 wt. % Y_2O_3 LA phonons in the [ζ00] direction.

though the nonstoichiometry creates vacancies in the oxygen sublattice. The frequencies and linewidths of the TA and LA phonons propagating along the principal symmetry directions [100], [110], and [111] in cubic zirconia have been measured as a function of temperature up to 1700 K using inelastic neutron scattering. No optical-phonon modes were observed. The experimentally obtained TA and LA phonon dispersion curves of ZrO_2–20 wt. % Y_2O_3 at 300 K have been fitted by a rigid-ion-model[11,12] calculation. Values of the main parameters relevant to the rigid-ion model used—such as lattice constant, TO and LO frequencies, F_{2g} Raman frequency—are tabulated here. The density of vibrational states is predicted and is used for speculating about the disorder introduced into the oxygen sublattice by the vacancies. Raman data and the optical branches investigated by inelastic neutron scattering appear to be particularly sensitive to this aspect.

In addition to the high-temperature (300–1700 K) inelastic neutron-scattering measurements, the diffuse-elastic-scattering investigations were also undertaken on ZrO_2–15 wt. % Y_2O_3 over the same temperature range.

II. EXPERIMENTAL PROCEDURE

The triple-axis spectrometer IN3 at Institute Laue-Langevin (ILL), Grenoble was used to determine the phonon dispersion curves in the $ZrO_2 \cdot Y_2O_3$(20 wt. %) at room temperature and ZrO_2–Y_2O_3(15 wt. %) from 300–1700 K.

X-ray crystallography was utilized for orienting the two samples; both the ZrO_2 containing 15 and 20 wt. % Y_2O_3 displayed a perfectly ordered fcc structure for the cation sublattice. This was later confirmed in the neutron-scattering studies. The crystals possessed only small mosaic spreads ($<0.1°$) as determined by analysis on a γ-ray diffractometer. Data were collected by a series of constant-Q or constant-energy scan in the high-symmetry directions [ζ00], [ζζ0], and [ζζζ] from the Brillouin-zone center toward the zone boundaries. The crystals (about 10 mm diameter and 40 mm in length) were mounted with the [011] plane horizontal. For the high-temperature studies the sample was mounted in a vacuum furnace.

The investigations on IN3 used monochromators of pyrolytic graphite (PG) (002) and Cu(111) with fixed incident energies; the scattered neutron beam was analyzed by a second PG (002) crystal and detected by a mul-

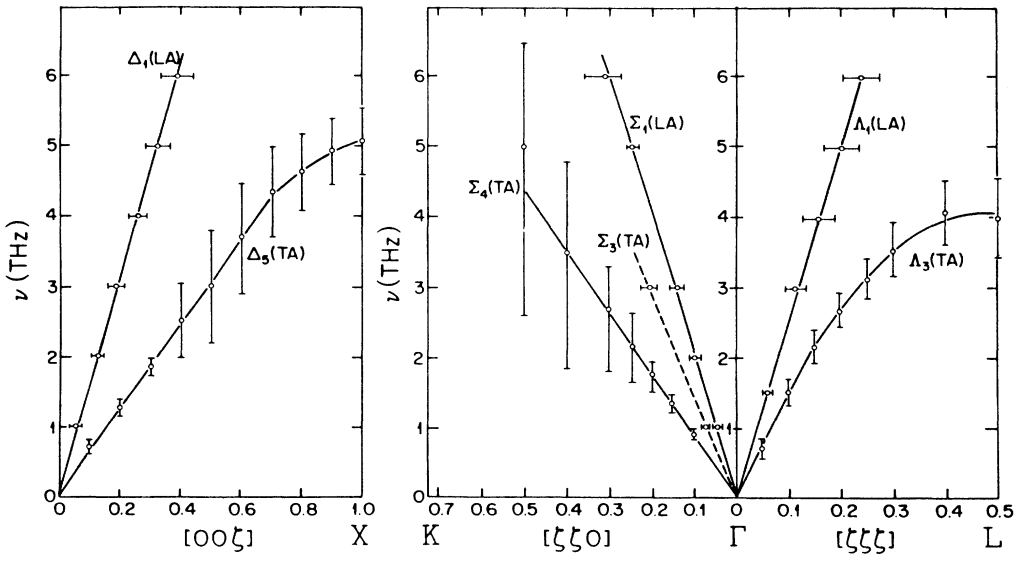

FIG. 3. A composite of all dispersion curves measured for ZrO_2–20 wt. % Y_2O_3 at 300 K; the bars represent the Lorentzian width FWHM determined from the fits in Figs. 1 and 2. No optical-phonon modes were observed.

tidetector consisting of 24 vertical ^{3}He tubes in three staggered rows. Collimation angles of 20′-20′-20′ were used before the monochromater, sample analyzer, and detector, respectively. An energy resolution of 0.10 meV [full width at half maximum (FWHM)] was determined from a vanadium sample which was used for calibration and normalization purposes. As the "resolution ellipsoid"[13–15] is optimally "focused" when the shortest axis of the ellipsoid is approximately normal to the dispersion surface, constant-Q scans were found more suitable for measuring the TA phonons, while constant-E scans were used for the LA phonons. The representative data for the direction [ζ00] are displayed in Figs. 1 and 2 for the TA and LA modes, respectively. ζ is the reduced phonon wave-vector component, and ν is the frequency in THz($=2\pi\zeta/a$). The phonon line shapes as a function of ζ and ν were assumed to be Lorentzian in form and were fitted for each scan as shown by the solid lines. The projection of these peaks in the ζ-ν plane are shown in Fig. 1 for the TA branches and in Fig. 2 for LA branches. The dotted lines in the figures represent the peak positions and show the dispersion branches. Figure 3 shows a composite of all dispersion curves measured; the bars represent the Lorentzian width (FWHM) determined from the fits in Figs. 1 and 2.

III. RESULTS AND DISCUSSION

The densities quoted in Table I were calculated from values of the lattice constants determined from the positions of Bragg peaks during the experiment. The cubic elastic constants C_{11}, C_{12}, and C_{44} given in Table I were derived from the slope of each acoustic branch in the linear dispersion region.[16] From the room-temperature results of ZrO_2–20 wt.% Y_2O_3 the following conclusions were reached.

(a) The phonons rapidly broadened in most directions and were poorly defined at large wave vectors near the zone boundaries. Dickens *et al.*[17] found that in their neutron-scattering studies of PbF_2 as a function of temperature, the TA phonons had linewidths proportional to q^2, approximately independent of direction at $T\sim570$ K. From this result they implied that their measurements were taken in the hydrodynamic regime in this temperature range. We observed similar behavior in the cubic zirconia samples even at room temperature. For example, all the TA branches showed a linewidth dependence $\propto q^2$ for $\zeta<0.55$, in accordance with a phenomenological viscous damping model[18] if the oxygens are considered to exhibit uncorrelated "fluidlike" motion about their site centers. The slope (Γ/ζ^2) of TA[$\zeta\zeta\zeta$] and the TA[ζ00] in cubic zirconia are almost the same ($\sim$40 THz A^2). These 300-K values are considerably larger than those obtained by Dickens *et al.*[17] for PbF_2 at 900 K.

(b) The measured elastic constants C_{11}, C_{12}, and C_{44}, density, and anisotropy factor A (defined as $[2C_{44}/(C_{11}-C_{12})]$) obtained from the neutron data proved to be in excellent agreement with those reported by Chistyi *et al.*[19] from Brillouin scattering studies, Leung[20] from ultrasonic studies, and Ingel[21] from densi-

TABLE I. Density, lattice constants, cubic elastic constants (units of 10^{12} dyn/cm^2), anisotropy factor (A), ionicity factor (B), and Cauchy factor (C) derived from the inelastic scattering data for two compositions of ZrO_2-Y_2O_3 and several temperatures. $A=2C_{44}/(C_{11}-C_{12})$, $B=C_{11}/C_{12}$, $C=C_{12}/C_{44}$.

	T (K)	Density (g/cm^3)	Lattice constant (Å)	C_{44}	C_{11}	C_{12}	A	B	C
20 wt.% Y_2O_3	300	5.91±0.01	5.15±0.01	0.60±0.01	3.91±0.03	1.20±0.05	0.32±0.03	3.26±0.05	2.00±0.05
15 wt.% Y_2O_3	300	5.98	5.15	0.61	4.75	1.44	0.36	3.30	2.36
	1000	5.85	5.19	0.53	4.43	1.17	0.33	3.78	2.21
	1700	5.71	5.23	0.45	3.99	1.02	0.31	3.91	2.27

ty measurements (samples used by Leung and Ingel were from the same source).

(c) No optical phonons were observed in these measurements. The optical branches result primarily from the out-of-phase motions of the two oxygen sublattices with respect to the zirconium sublattice. Raman data as a function of temperature[3-5] indicated that the oxygen sublattice was "disordered." The "random" fluctuations in the oxygen sublattice and a subsequent breakdown of wave-vector considerations does not allow well-defined optic-phonon branches to be observed in the inelastic neutron scattering. The acoustic modes, on the other hand, are due to primarily the in-phase of motion between the oxygen and cation sublattices; the much heavier and perfectly ordered fcc zirconium sublattice is the main contributor to the vibrational motion associated with the acoustic-phonon modes. As a consequence, it is possible to observe the acoustic modes even though they are highly damped (large FWHM). Detailed interpretation of this interesting result requires further experimental and theoretical investigations.

A rigid-ion model[12] was utilized to generate the unobserved optical-phonon-mode branches. The parameters for the model are given in Table III. The three independent elastic constants C_{11}, C_{12}, and C_{44} were obtained experimentally from the slopes of acoustic branches in the linear dispersion region. Kramers-Kronig analysis[22,23] of our infrared reflection measurements provided the zone center ω_{TO} and ω_{LO} frequencies at 320 ± 10 and 705 ± 10 cm^{-1}, respectively. The zone-center Raman frequency of F_{2g} symmetry is unknown due to the disorder of the oxygen sublattice; it was found to be one of the most sensitive parameters associated with the best fit to all the experimentally available acoustic dispersion branches.

The value of the Raman frequency has been ambiguous and the subject of considerable controversy due to the disorder in the oxygen sublattice. However, the fitting of the acoustic dispersion branches determined by inelastic neutron scattering provided the most reasonable Raman frequency ω_R (585 cm^{-1}); the other five parameters C_{11}, C_{12}, C_{44}, ω_{TO} and ω_{LO} were allowed to float around the values obtained experimentally.

Table II lists the best-fit parameters along with their corresponding experimental values. Table III shows the effective charge Z and the short-range force constants α_1, β_1, β_2, γ_2, and α_3 obtained from the rigid-ion-(RI) model calculation. The RI model results for UO_2 and CaF_2 are shown for comparison. The elastic constants for ZrO_2–20 wt.% Y_2O_3 are comparable with those found for UO_2,[8,24] and are about twice as large as those obtained for CaF_2.[12,25]

The dispersion curves generated from the rigid-ion model are given in Fig. 4 for the high-symmetry directions $[\zeta00]$, $[\zeta\zeta0]$, and $[\zeta\zeta\zeta]$, Figure 5 displays the calculated frequency distribution of the one-phonon density of states for ZrO_2–20 wt.% Y_2O_3. Comparisons are made in the same figure between the phonon density of states and reduced Raman spectrum. The marked resemblances between the calculated and measured spectra confirm the disordering in the oxygen sublattice of cubic zirconia.

The same inelastic neutron-scattering procedures were applied on $ZrO_2 \cdot Y_2O_3$(15 wt.%) sample. In addition to the room-temperature studies, measurements were also taken at 1000 and 1700 K. As expected, a softening of the dispersion curves and a concomitant decrease in the elastic constants was found as the temperature increased (Table I). The $\Gamma \propto \zeta^2$ relationship still holds for the TA branches but no significant change in Γ at a specific ζ was observed from room temperature up to 1700 K. In the hydrodynamic regime of a system with two charged sublattices of which one is mobile (in our case the oxygen sublattice) and the other one is fixed (the Zr sublattice), the Zeyher's treatment of the damping is given by $(D+\eta)\zeta^2/2$ where η is the viscosity coefficient, arising from damping due to anharmonicity, and D is proportional to the ionic conductivity which is an exponential temperature-dependent function.[26] Due to the insensitivity of the phonon width with the temperature it appears that the hopping motion of the oxygen ions in this ionic conducting crystal makes only a small contribution

TABLE II. Rigid-ion-model parameters for ZrO_2–20 wt.% Y_2O_3 obtained from the fits shown in Fig. 4, along with their corresponding experimental values. RI model results for UO_2 and CaF_2 are shown for comparison. * represents a result that was not observable due to the disordering in the oxygen sublattice.

	ZrO_2–20 wt.% Y_2O_3			
	RI model	Experimental	UO_2	CaF_2
ω_R (cm^{-1})	580–590	*[a]	467[b]	312[c]
ω_{TO} (cm^{-1})	310	320±10[a]	278[b]	267[c]
ω_{LO} (cm^{-1})	690	705±10[a]	556[b]	472[d]
C_{11} (dyn/cm^2)	38.0×10^{11}	39.1×10^{11}	40.3×10^{11}[e]	17.4×10^{11}
C_{12} (dyn/cm^2)	13.0×10^{11}	12.0×10^{11}	14.2×10^{11}[e]	5.6×10^{11}
C_{44} (dyn/cm^2)	5.9×10^{11}	6.0×10^{11}	6.9×10^{11}[e]	3.59×10^{11}
ϵ_∞		4.67	5.3	2.047
$r=a/2$ (Å)		2.575	2.734	2.725

[a]Reference 5.
[b]Reference 24.
[c]Reference 12.
[d]Reference 25.
[e]Reference 8.

TABLE III. Short-range force constants and effective charge for ZrO_2–20 wt. % Y_2O_3, UO_2, and CaF_2 based upon rigid-ion-model calculations. Values in columns two through four are in units of e^2/r^3.

	ZrO_2–20 wt. % Y_2O_3	UO_2	CaF_2
Z^2	1.56	1.36	0.609
α_1	2.88	2.85	1.537
β_1	4.66	6.21	2.707
β_2	−0.49	1.58	0.315
γ_2	0.07	0.41	0.274
α_3	3.00	1.71	1.079

to the total width, while the intrinsic defects and anharmonicity predominate the damping mechanism. A similar conclusion arrived at the diffuse elastic studies discussed in the next section.

IV. DIFFUSE ELASTIC NEUTRON SCATTERING

Diffuse-elastic-scattering measurements were also undertaken on IN3. It was found that in addition to the expected Bragg scattering, which is located at the Brillouin-zone centers of reciprocal-lattice space, the scattering density varied with Q displaying marked contours a shown in Fig. 6. Broad intensity peaks were observed in anisotropic shells located around (1 1.75 1.75) and (3.8 0.9 0.9) for the ZrO_2–20 wt. % Y_2O_3 at room temperature (Fig. 6). The distances to the $\Gamma(000)$ point from these two broad peaks are 2.67 and 4.0 in reciprocal-space units ($2\pi/a$), respectively. Their ratio of 1.49 is possibly related to the two different distances of adjacent oxygen atoms in oxygen sublattice $\{110\}$ plane (ideally in a cubic fluorite structure this is $\sqrt{2}$:1). However, the investigations were too limited to infer if the diffuse scattering showed periodicity in reciprocal-lattice space.

Similar studies were made for the ZrO_2–15 wt. % Y_2O_3 sample at 300, 1000, and 1700 K in the vacuum furnace. In comparison with the results for 20 wt. % Y_2O_3, the broad peaks were located at slightly different positions at (0.9 1.8 1.8) and (3.9 1.0 1.0) at 300 K. Nevertheless, the overall contour patterns of two broad intensity regions were almost identical. The intensity contour map of cubic zirconia (ZrO_2–15 wt. % Y_2O_3) showed almost no change on raising the temperature up to 1700 K, and no quasielastic scattering was observed.

Our results imply that the static deformation of the oxygen sublattice due to the vacancies remains almost temperature independent up to 1700 K. These results substantiate a model of static structural disorder in the oxygen sublattice, as such diffuse scattering most likely stems from lattice deformations caused by the oxygen vacancies in the $ZrO_2 \cdot Y_2O_3$ sample. Steel and Fender[27] also concluded that the oxygen sublattice does have a static structure disorder for $ZrO_2 \cdot Y_2O_3$ (15–22 wt. %) system. It should be pointed out that some variations in intensity with Q are expected due to absorption and the Debye-Waller factor,[28] but these are estimated to be small in comparison to the observed intensity contours of their temperature dependence.

Diffuse elastic scattering on $SrCl_2$ was carried out by Dickens *et al.*[29] The highest intensity was found near (2.3 0 0) and (1 2 2) on the reciprocal-lattice plane, where strong quasielastic scattering was observed above T_c (the superionic transition temperature). The striking similarity between the scattering intensity and the disorder heat content confirms that the origin of the quasi-

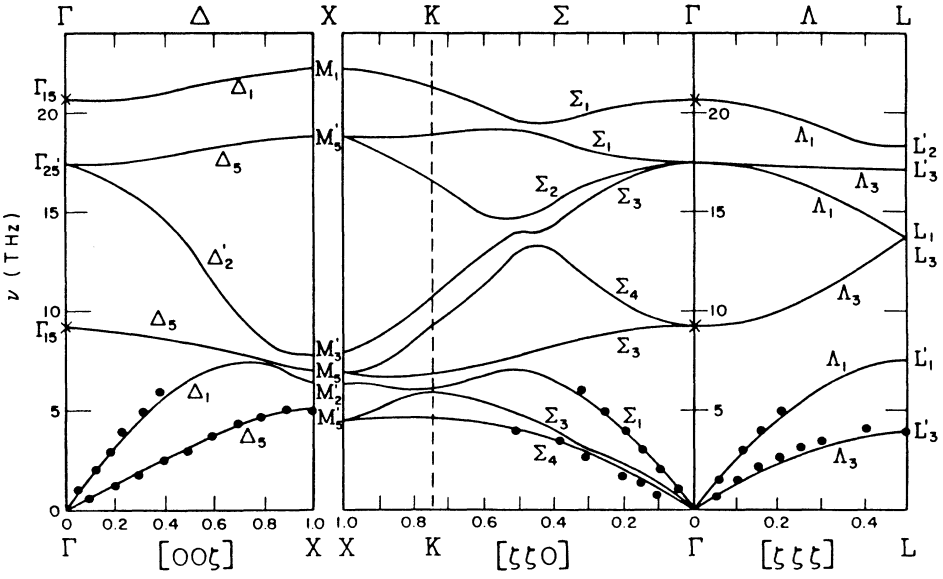

FIG. 4. The best-fit phonon dispersion curves for cubic zirconia (ZrO_2–20 wt. % Y_2O_3) in three directions of high symmetry, calculated based upon the rigid-ion model. The experimentally obtained acoustic modes are depicted by solid circles; the ir optic modes by crosses.

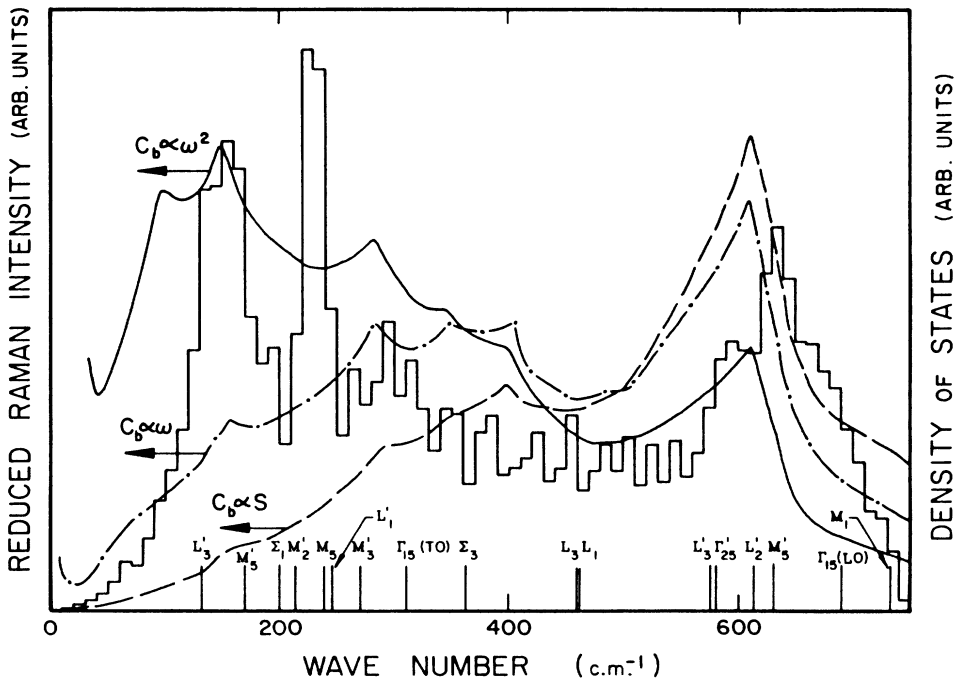

FIG. 5. Comparisons of the calculated one-phonon density-of-states histogram and the reduced Raman spectra for ZrO_2–20 wt. % Y_2O_3 [C_b = const, $C_b \propto \omega$, and $C_b \propto \omega^2$ utilizing the expression given by Shuker and Gamon (Ref. 7)].

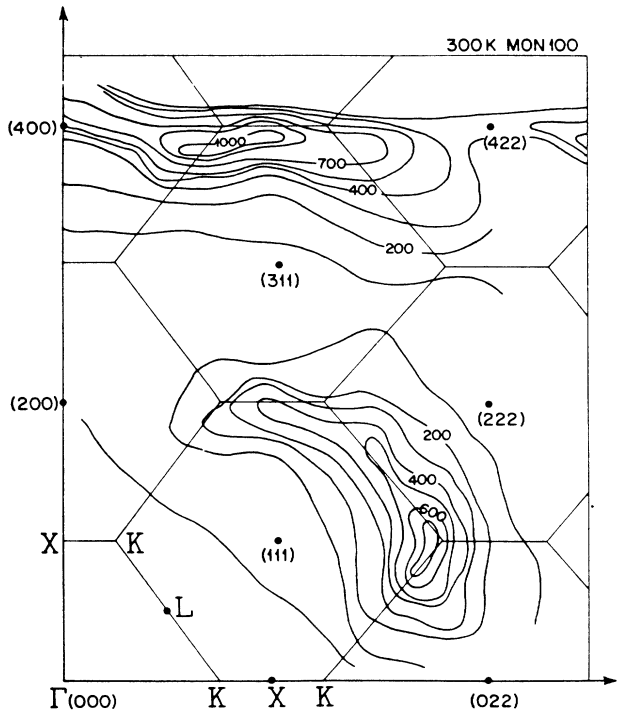

FIG. 6. Elastic diffuse scattering distribution of the intensities over the reciprocal-lattice plane for ZrO_2–20 wt. % Y_2O_3 at 300 K. In addition to the expected Bragg scattering, which is located at the Brillouin-zone centers of the reciprocal lattice, broad intensity peaks were observed in the anisotropic shell located around (1 1.75 1.75) and (3.8 0.9 0.9).

elastic scattering is directly related to "dynamical" disordering in the $SrCl_2$ lattice.

In contrast there is no indication that a transition temperature, as is observed in $SrCl_2$, exists in cubic zirconia at least up to 1700 K. In contrast with this negative result, quasielastic light scattering was observed in cubic zirconia at high temperatures (600–1500 K), and has been identified as a disorder-order transition.[30]

V. CONCLUSION

The frequencies and linewidths of the TA and LA phonons propagating along the three principal symmetry directions in fully stablized cubic $ZrO_2 \cdot Y_2O_3$ have been measured as a function of temperature up to 1700 K. However, no branches corresponding to the optical phonons could be observed. Raman spectrum essentially reflects the frequency distribution of the density of states obtained from a "rigid-ion" calculation. In was determined that the Raman frequency (F_{2g} mode) could be estimated at 585 cm^{-1} when considering best-fit results to the measured acoustic branches. Diffuse elastic scattering was extensively mapped in the reciprocal space over the same temperature range. Broad intensity peaks were observed in anisotropic shells located around (1 1.75 1.75) and (3.9 1 1). No superionic transition temperature T_c was observed in this superionic conductor–cubic-zirconia system over the temperature range investigated.

ACKNOWLEDGMENTS

The single-crystal samples were grown by the Ceres Corporation and we wish to thank J. F. Wenkus and R. P. Menashi for their continued interest in this work. The work at Northeastern University was supported by the United States Department of Energy under Grant No. EE-FG02-84ER45079.

---

*Present address: Department of Physics, Florida Atlantic University, Boca Raton, Florida 33431-0991.

†Present address: AT&T Bell Laboratories, 1600 Osgood Street, North Andover, Massachusetts 01845.

[1]A. H. Heuer, F. F. Lang, M. V. Swain, and A. G. Evans, J. Am. Ceram. Soc. **69**, No. 3 (1986).

[2]A. H. Heuer and L. W. Hobbs, Science and Technology of Zirconia, Advances in Ceramics (The American Ceramics Society, Inc., Columbus, Ohio, 1981), Vol. 3.

[3]C. H. Perry, D. W. Liu, and R. P. Ingel, J. Am. Ceram. Soc. **68**, C184 (1985).

[4]A. Feinberg and C. H. Perry, J. Phys. Chem. Solids **42**, 513 (1981).

[5]D. W. Liu, Ph.D. thesis, Northeastern University (1984).

[6]R. Loudon and W. Hayes, *Scattering of Light by Crystals* (Wiley, New York, 1978).

[7]R. Shuker and R. W. Gammon, Phys. Rev. Lett. **25**, 222 (1970).

[8]G. Dolling, R. A. Cowley, and A. D. B. Woods, Can. J. Phys. **43**, 1397 (1965).

[9]J. D. Axe and G. D. Pettit, Phys. Rev. **151**, 676 (1966).

[10]V. I. Aleksandrov, V. A. Osiko, A. M. Prokhorov, and V. M. Tatarintesev, Current Topics in Material Science, edited by E. Kaldis (North-Holland, Amsterdam, 1978), Vol. 1, pp. 421–480.

[11]S. Ganesan and R. Srinivasan, Can. J. Phys. **40**, 74 (1962); **40**, 91 (1962).

[12]W. B. Lacina and P. S. Pershan, Phys. Rev. B **1**, 1765 (1970).

[13]M. J. Cooper and R. Nathans, Acta Crystallogr. **23**, 357 (1967).

[14]R. Stedman and G. Nilsson, Phys. Rev. **145**, 492 (1966).

[15]M. Nielsen and H. Bjerrum Moller, Acta Crystallogr. Sect. A **25**, 547 (1969).

[16]C. Kittel, *Introduction to Solid State Physics*, 2nd Ed (Wiley, New York, 1956), Chap. 2.

[17]M. H. Dickens, W. Hayes, M. T. Hutchings, and W. G. Kleppman, J. Phys. C **12**, 17 (1979).

[18]L. D. Landau and E. M. Lifshitz, Theory of Elasticity (Pergamon, New York, 1975), Vol. 7, Chap. 5.

[19]I. L. Chistyi, I. L. Fabelinskii, V. F. Kitaeva, V. V. Osiko, Yu V. Pisarevskii, I. M. Sil'vestrova, and N. N. Sobelev, J. Raman Spectrosc. **6**, 183 (1977).

[20]R. Leung (private communication).

[21]R. Ingel and D. Lewis, J. Am. Ceram. Soc. (to be published).

[22]J. R. Jasperse, A. Kahan, and J. N. Plendl, Phys. Rev. **146**, 526 (1966).

[23]Pamela Denham, G. R. Field, P. L. R. Morse, and G. R. Wilkinson, Proc. R. Soc. London, Sec. A **317**, 55 (1970).

[24]V. G. Keramidas and W. B. White, J. Chem. Phys. **59**, 1561 (1973).

[25]J. Faber, M. H. Muller, and B. R. Cooper, Phys. Rev. B **17**, 4884 (1978).

[26]M. Kleitz, H. Bernard, E. Fernandez, and E. Schoulder, *Science and Technology of Zirconia, Advances in Ceramics* (The American Ceramics Society, Inc., Columbus, Ohio, 1981), Vol. 3, pp. 310–336.

[27]D. Steel and B. E. F. Fender, J. Phys. C **7**, 1 (1974).

[28]G. L. Squares, *Introduction to the Theory of Thermal Neutron Scattering* (Cambridge University Press, Cambridge, England, 1978), Chap. 3.

[29]M. H. Dickens, M. T. Hutchings, J. Kjems, and R. E. Lechner, J. Phys. C **11**, L583 (1978).

[30]D. W. Liu, C. H. Perry, W. Wang, and R. P. Ingel, J. Appl. Phys. **62**, 250 (1987).